



Quasi-optical assessment of the ALMA band 9 front-end

Massimo Candotti^a, Andrey M. Baryshev^b, Neil Trappe^{c,*}

^a National Astronomical Observatory of Japan 2-21-1 Osawa, Mitaka, Tokyo 181-8588, Japan

^b Kapteyn Astronomical Institute and Netherlands Space Research Organization, P.O. Box 800, 9700 AV Groningen, The Netherlands

^c National University of Ireland, Exp. Physics Dept., Maynooth, Co. Kildare, Ireland

ARTICLE INFO

Article history:

Received 19 January 2009

Available online 22 July 2009

Keywords:

Quasi-optical systems

Antenna

Near-field beam pattern measurements

Physical optics simulations

ABSTRACT

The ALMA band 9 (600–720 GHz) receiver is a dual channel heterodyne system which is capable of detecting orthogonally polarised signals utilising a wire grid beam splitter. Two Superconductor–Insulator–Superconductor (SIS) mixers mounted behind hybrid mode corrugated horns are coupled to the 12 m Cassegrain antenna via a wavelength independent configuration of two off-axis elliptical mirrors.

We outline an approach involving accurate physical optics simulations in conjunction with precise experimental measurements of the complete optical front-end which guarantees the highest performances. This practical verification approach can be generalised to all quasi-optical receivers to validate system performance. In this paper, we verify the optical design and estimate antenna system efficiency. Comparison between measurement and simulation indicates precise information is achievable in estimating system performance allowing potential improvements in ALMA instrument calibration accuracy.

© 2009 Elsevier B.V. All rights reserved.

1. Introduction

ALMA is a mm/sub-mm radio-interferometer instrument consisting of 50+ antennas [1]. Each of the Cassegrain antennas will host an individual cryostat housing 10 independent cartridges, each of them containing a dedicated heterodyne receiver for a selected band of interest [1]. The ALMA band 9 cartridge, which covers the range 600–720 GHz, is cryogenically cooled and contains a dual polarised front-end with local oscillator quasi-optical coupling system. In this paper we outline a full description of this quasi-optical design and analysis of the band 9 front-end, and in the Appendix A we report a brief description of the experimental set-up used to verify its operation with precise beam pattern amplitude and phase planar scans. We include a parallel analysis of using physical optics simulations, a vital aspect of the overall verification process. Both simulated and experimental data are used to estimate antenna efficiency and co-alignment of the orthogonally polarised beams on the sky. We draw conclusions on the verification process used and then summarise the results in relation to the ALMA project specifications.

2. ALMA band 9 front-end

2.1. ALMA antenna configuration

For the overall ALMA configuration, detailed studies have been comprehensively carried out in order to choose the optimum opti-

cal configuration most suitable for a 50 antenna interferometer [2–6]. The final 12 m Cassegrain antenna design is discussed and verified in [7] and is used as a basis in the analysis presented here. The ALMA Cassegrain final optical configuration is characterised by a long f_e/D ratio equal to 8, which allows a cryostat with ten receivers to be located in the telescope focal plane, 1377 mm below the primary vertex. The distance from the Cassegrain focus to the secondary mirror vertex is 5883 mm [7].

2.2. Design of the mirror coupling system

The mirror coupling system has been designed to maximise antenna efficiency in a wavelength independent manner over the entire band from 600 to 720 GHz [8]. The maximisation of the illumination and spillover efficiency is obtained by designing the tertiary optics to produce a beam edge taper at the secondary mirror of -12 dB [9]. The use of corrugated horns to feed the mixer device, guarantees a predictable symmetric beam with 98% power coupling to the fundamental Gaussian, which was initially used in the optical design [10]. Furthermore, the corrugated horn feed has a potentially low cross-polar component, which also contributes to the optimum front-end design. Considerable efforts have been made in order to design a compact quasi-optical system which mechanically fits inside the limited space of the 4 K stage of the ALMA band 9 cartridge still meeting the difficult efficiency goals described above [11].

A schematic of the optical design is shown in Fig. 1 with the two off-axis mirrors M3 and M4 for the signal path (M1 and M2 are the Cassegrain primary and secondary mirrors). M3 focuses radiation towards the secondary reflector and is located 150 mm from the

* Corresponding author. Tel.: +353 17084658.

E-mail address: neal.a.trappe@nuim.ie (N. Trappe).

nominal Cassegrain focal plane. The simultaneous detection of orthogonal polarisations of astronomical signals is achieved quasi-optically by means of a wire grid polariser located between M3 and M4 as orthomode transducers are difficult to implement at such high frequency ranges. This beam splitting grid also defines an axis of symmetry where the two signal polarisation configurations are separated, as illustrated in Fig. 1 section A–A' and B–B'. Polarisation OP is designated the reflected component from the grid wires which are parallel to the direction of the horn axes (see Fig. 1 section B–B').

Polarisation 1P on the other hand is the component transmitted through the wire grid. The common mirror labeled M3, is used to redirect both polarisation beams towards the sub-reflector mirror with an off-set angle of 0.974° (see Fig. 1 section A–A'). Fig. 1 section A–A' and C–C' also outline how the quasi-optical LO injection is achieved using two further off-axis ellipsoidal mirrors (M5 and M6 176 mm apart). The local oscillator feed source is a diagonal horn providing a 84% power coupling factor of the co-polar component with a symmetric fundamental Gaussian [10]. This allows good LO coupling to the mixer corrugated horn over the channel bandwidth with an easy-to-make LO horn. The beam splitter used to inject a fraction of the local oscillator power signal into the mixer horn is a $12\ \mu\text{m}$ thin film made of Mylar. More information about the optics geometry layout is available at [11].

3. Quasi-optical analysis

As stated already the high Gaussianity properties of a corrugated horn allows one to initially validate the optical design by using fundamental mode Gaussian ABCD matrix analysis techniques [10,12,13]. The complex beam ray tracing model for the signal path is based on the inter-component distances and phase transformer focal lengths, i.e. the ellipsoidal mirror focal lengths reported in [11]. It comprises of a beam transfer matrix describing the optical system from the mixer horn to the telescope sub-reflector as shown in the schematic of Fig. 2, where the components are treated in transmission. The ABCD analysis reported in Table 1 shows that a $-12.87\ \text{dB}$ edge taper at the secondary plane is achieved over the entire bandwidth of ALMA band 9. This indicates the sub-reflector is over illuminated in comparison to the $-12\ \text{dB}$ edge taper rule. This is due to the fact that at the time of the design a distance from sub-reflector to focal plane of 6000 mm was adopted rather than the nominal distance of 5883 mm. For a more detailed analysis of the beam propagation through the optical system, accurate electromagnetic simulations were also carried out using a vector physical optics approach applied to a complete geometrical model of the optical system including the actual mechanical rims of the mirrors. In addition, a full electromagnetic description of the corrugated horn is included using a modematching technique to describe the horn aperture field in terms of co and cross-polar field components. The software predictions represent the ideal performance of the optical system at a predetermined comparison plane of measurement. Equivalent measurements have been taken for both polarisation signals (OP and 1P), at the same location close to the telescope focal image plane, see Fig. 1 left corner. As the alignment and positioning of the experimental set-up are accurate to micron scales using a precise theodolite autocollimation operation of mechanical reference points on the scanner and optical structures (see the Appendix A section), the experimental and simulated beam patterns can be compared precisely. The tolerance and experimental accuracy of the system is summarised in Table 5 in the Appendix A. To compensate for standing waves in the scanning system, two measurements are made at each point in quick succession separated by half a wavelength and averaged. This corrects, at least to the first order, the influence of reflected power in the system. Phase drift in the system is not significant for 1D cuts with a short scan time and this linear drift effect is easily corrected for longer 2D scans if necessary. The reproducibility of the measurements is excellent with the system producing beams that vary less than $-60\ \text{dB}$ between scans. For the simulations, the equivalent plane of measurement is easy to implement allowing close comparison of theory and experiment. For both, experimental measurements and software simulations, the location of the comparison grid is a plane normal to the telescope axis with the centre of the coordinate system located 145 mm in front of the chief ray intersection point on M3 (dotted line in Fig. 1 section A–A').

3.1. Signal path analysis

In Fig. 3 we illustrate the agreement between physical optics simulation and precise measurement of the beam at a plane close to the Cassegrain focal plane for two orthogonal cuts ($E = 0^\circ, H = 90^\circ$) of the OP and 1P polarisation. Measurements were made at 668 GHz, close to the central frequency 661 GHz. The dB intensity and phase plots illustrate remarkable agreement between simulation and measurement to low levels where side lobes are reproduced to the order of -50 or $-60\ \text{dB}$. The phase plots are agree well over the main beam and reproduce the characteristic phase jumps at equivalent off-axis distances.

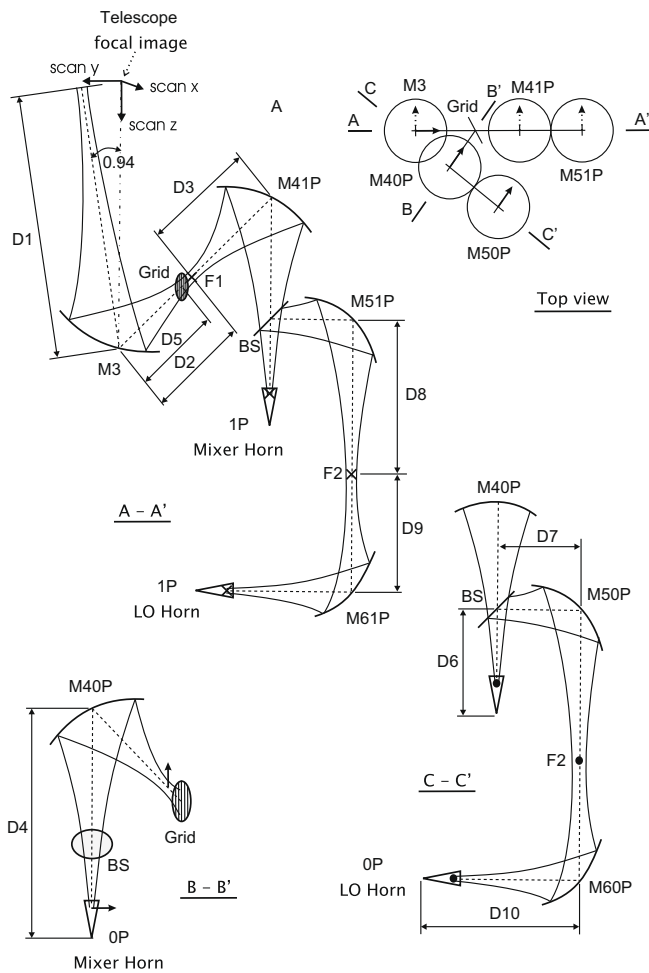


Fig. 1. ALMA band 9 optical coupling configuration. The LO power injection is achieved quasi-optically by means of Mylar beam splitters (labelled BS). The continuous line arrow and black spot indicate the OP signal polarisation and the dashed line arrow and black cross represent the 1P. Drawings not in scale.

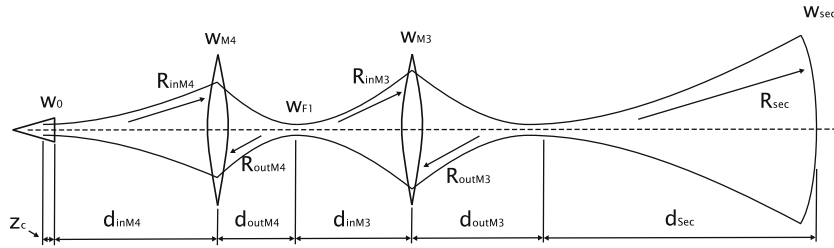


Fig. 2. ALMA band 9 ABCD analysis scheme for the signal path. The secondary is located at the nominal optical configuration distance of 5883 mm. The parameter z_c is the distance from the horn aperture back to the horn phase centre.

Table 1

Band 9 signal ABCD analysis at the frequencies of 600, 661 and 720 GHz. z_c corresponds to the distance from the horn aperture to the phase centre located behind the aperture. The ABCD parameters refers to the scheme shown in Fig. 2.

Parameter	Frequency (GHz)		
	600	661	720
z_c (mm)	8.42	9.15	9.80
d_{inM4} (mm)	44.42	44.42	44.42
d_{outM4} (mm)	45.33	44.92	44.58
d_{inM3} (mm)	50.57	50.99	51.33
d_{outM3} (mm)	149.27	149.26	149.26
d_{Sec} (mm)	5883.64	5883.64	5883.64
R_{inM4} (mm)	54.01	54.70	55.30
R_{outM4} (mm)	-46.06	-45.58	-45.17
R_{inM3} (mm)	51.23	51.57	51.84
R_{outM3} (mm)	-170.81	-167.12	-164.30
R_{Sec} (mm)	5884.92	5884.84	5884.78
w_0 (mm)	1.12	1.06	1.00
w_{M4} (mm)	7.58	7.37	7.20
w_{OF1} (mm)	0.95	0.89	0.82
w_{M3} (mm)	8.44	8.35	8.28
w_{OFp} (mm)	3.00	2.73	2.51
w_{Sec} (mm)	311.17	311.16	311.16
T_{eSec} (dB)	-12.87	-12.87	-12.87

From 2D amplitude and phase beam pattern measurements (and simulations) it is possible to retrieve information about beam quality, i.e. the degree of Gaussicity [14]. This is achieved by fitting a Fundamental Gaussian Beam Mode (FGBM) to the beam pattern. The results of this analysis are reported in Table 2 for both simu-

lated and measured data for both polarisation configurations at a central frequency of 668 GHz. We analyse the beam at the measurement location in terms of Gaussicity, beam radii (w_{0x}, w_{0y}), the off-sets from beam centre and tilts in each direction ($x_0, y_0, x_{tilt}, y_{tilt}$) and equivalent distance to waist position z_0 . The agreement between the theoretical model and the experimental results is very good for polarisation 1P, while on the other hand comparisons between theoretical predictions and experimental measurements for the OP configuration show that the experimental beam, points in an off-set direction away from the designed direction.

This suggests that there could be a misalignment issue within the optical parts constituting the front-end, highlighting what the impact of a correct tolerance budget can have on high-performing quasi-optical reflector system.

4. Antenna performance

The main beam predictions of the measured data propagated towards secondary and primary reflectors are reported in Fig. 4. The plots show azimuth and elevation cuts for both OP and 1P polarisation configurations; the azimuth cut being the plane containing the off-axis optical path. The main beam pattern distributions show first side lobes at less than -22 dB below the main peak. The beam symmetry is also good proving a correct illumination of the sub-reflector is obtained for each polarisation. This prediction of the beam pattern is achieved by propagating beam measurements taken at the telescope focal plane through an ideal (perfect phase transforming) telescope and on to the sky.

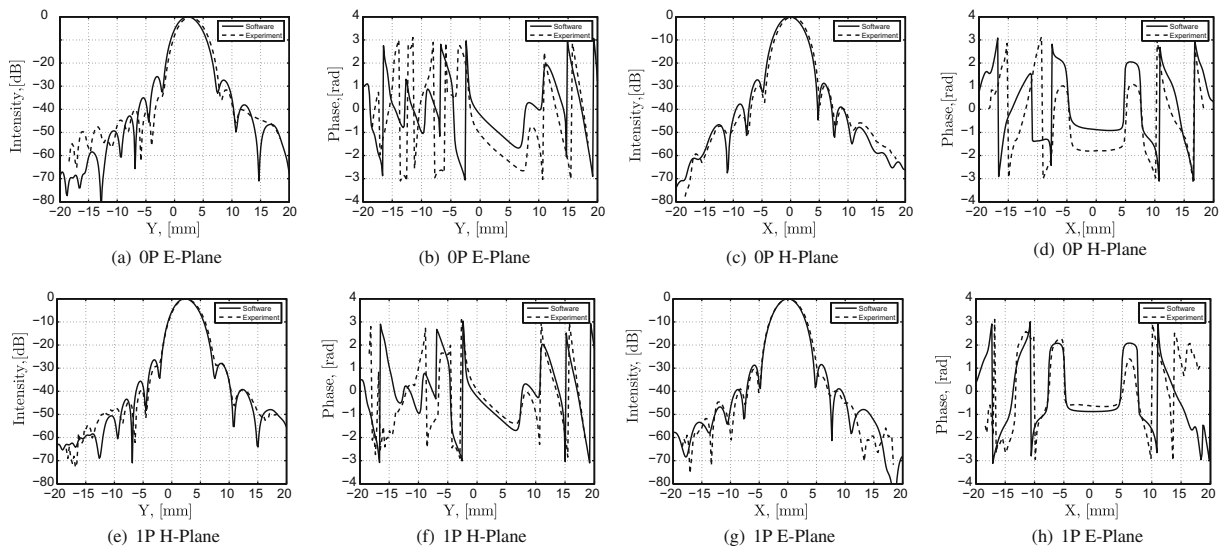


Fig. 3. Experimental and software comparison for the two polarisation beams at the focal plane. Frequency 668 GHz.

Table 2

FGBM fitting analysis for the two polarisation configurations at the telescope focal plane. $f = 668$ GHz, close to and consistent with band centre $f = 661$ GHz.

Parameter	Experimental		Software	
	OP	1P	OP	1P
Gaussicity (%)	98.31	98.17	97.98	98.19
w_{0x} (mm)	2.94	3.05	2.98	2.98
w_{0y} (mm)	2.96	2.95	2.98	2.97
x_0 (mm)	-0.26	0.00	0.10	0.00
y_0 (mm)	2.85	2.58	2.45	2.45
z_0 (mm)	-3.05	-4.35	-4.45	-3.79
x_{tilt} (°)	-0.04	0.06	0.14	0.00
y_{tilt} (°)	0.89	1.00	1.00	1.00

4.1. Aperture efficiency

In assessing the aperture efficiency, an approximate method was used as would normally be the case for large telescopes. Due to the large telescope diameter (in terms of wavelength) for the band 9 frequencies extremely lengthy simulations would need to be performed in order to calculate the electric field distribution at the main dish aperture plane. The method used here deals with the electric field distribution collected at the secondary plane only. The phase information, once unwrapped, is fitted with a quadratic term representing the principal phase front term. By subtracting this parabolic term from the phase distribution, the Cassegrain phase transforming operation is therefore reproduced in an ideal way. In this procedure the effects of diffraction and truncation of the field amplitude distribution at the sub-reflector edges and struts are not considered. The phase distribution is then flattened representing the phase front after reflection at the main dish aperture. This field distribution is used to evaluate the beam coupling efficiency with an ideal top-hat field distribution, taking into account the stretching factor for the secondary to primary dish obscuration. In Table 3, the total antenna efficiency calculated is broken down into the main components, from spillover, illumination and Ruze factor due to the ALMA antenna surface roughness of $20 \mu\text{m}$ [15,16]. At 600 GHz, the efficiency calculated for the measured data is lower than the equivalent theoretical predictions. This is not in agreement with the trend of the two other listed frequencies. The reason for this could be that the measured signal at 600 GHz was slightly saturated at the peak power levels. This artefact could have lead to a beam pattern distribution with lower coupling efficiency with a top-hat distribution compared to an unsaturated beam pattern distribution. The results in Table 3 are

Table 3

Aperture efficiency for the ALMA band 9 optical system evaluated for the software model (full GRASP PO simulation) and the near-field measurement used as source input into the antenna model.

f (GHz)	Efficiency	Software		Experimental	
		OP	1P	OP	1P
600	η_{ill}	87.93	87.70	82.67	81.51
	η_{bl}	99.66	99.65	99.60	99.63
	η_s	93.36	92.97	95.38	95.66
	η_{Ruze}	77.28	77.28	77.28	77.28
	η_{tot}	63.15	62.79	60.69	60.03
661	η_{ill}	81.82	81.75	80.36	83.45
	η_{bl}	99.66	99.66	99.66	99.65
	η_s	96.03	95.82	96.51	95.67
	η_{Ruze}	73.29	73.29	73.29	73.29
	η_{tot}	57.39	57.21	56.65	58.31
720	η_{ill}	78.79	79.28	73.55	73.87
	η_{bl}	99.68	99.68	99.65	96.66
	η_s	97.77	95.38	97.75	97.67
	η_{Ruze}	69.16	69.16	69.16	69.16
	η_{tot}	52.56	50.56	49.55	49.73

rather optimistic, of course, they show how the optical front-end is properly designed to couple with the Cassegrain antenna with efficiency values close to the theoretical ones for fundamental Gaussian secondary illumination. A conservative cross-polarisation value of 1% should also be taken into account in the whole antenna efficiency reported in Table 3.

4.2. Main beam squint

The band 9 dual orthogonally polarised beams are formed using of a wire grid. The two beams follow separate paths from the grid to the related feed horn. Displacement of the optical components can cause relative beam squint between the two main beams on the sky, potentially affecting the receivers calibration procedure. In fact when pointing the antenna to a calibrator source it is desirable that the two polarisation receivers have the same instrumental calibration. This is ensured if the two beams point at the same amplitude source calibrator observed at the centre of both main beams. Therefore, for comparable mapping of the two polarisation observations, it is important to have equivalent system calibration

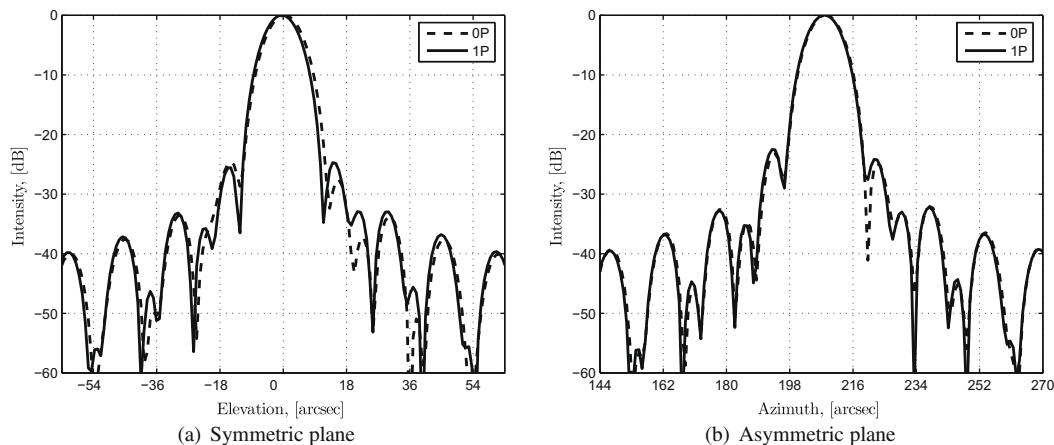


Fig. 4. Main beam prediction of ALMA band 9 at 661 GHz for the two polarisation beams retrieved from experimental measurements at the focal plane propagated to the sky, treating the telescope in an ideal phase transformer.

Table 4

Beam separation angle between the two polarisation main beams, OP and 1P configurations. The results are obtained from direct PO computation.

f (GHz)	Software	Experimental
600	0.13"	0.69"
661	0.13"	0.77"
720	0.14"	0.45"

for both receivers. The specification for the ALMA project imposes a 1/10 Half Power Beam Width (HPBW) restriction on beam misalignment. For band 9 the two polarisation beams on the sky are presented in Fig. 4 on the sky. The two beams obtained from the propagation toward the Cassegrain system of the measured data at the focal plane, are visibly not overlapped on the sky. Using the far-field main beam predictions, the separation beam angle can be calculated by fitting a fundamental Gaussian and evaluating the beam centre displacements of the OP and 1P fitted Gaussians.

By using the concept of image scale it can be shown that the angular beam separation on the sky θ , is directly related to the linear beam separation at the Cassegrain focal plane d_{FP} . The image scale factor of a telescope is given by

$$d_{FP} = \frac{f_e}{206265} \theta, \quad (1)$$

where f_e is the equivalent focal length of the Cassegrain system which is given by the product of the equivalent f -number and primary diameter D_p . Eq. (1) is valid for linear distances in mm and separation angle in arcseconds. This simple relation gives a good first approximation to the beam separation angle on the sky, knowing the beam separation in the focal plane. Therefore, the beam squint on the sky can be estimated from focal plane beam measurements. This can be shown for the case of focal plane measurements shown in Table 2. It is seen that the two polarisation beams are separated from each other by 0.37 mm in the xy focal plane. The beam deviation angle on the sky is $0.80''$, or 9.2% of the HPBW using Eq. (1). This result is very close to the one using detailed PO analysis, as shown in Table 4 indicating the approximate method is valid.

Table 5

Main features of the SRON near-field measurement facility for the quasi-optical assessment of the ALMA band 9 front-end optics.

Electrical parameter	Unit	Value
Frequency of operation	GHz	600–720
Signal to noise ratio (SNR)	dB	60
IF bandwidth B	Hz	10
Integration time τ	s	0.1
Amplitude stability	%/h	± 2
Phase stability	deg/h	± 20
Residual gain compression	dB	< 0.3
Typical 1σ main beam ampl. error	dB	0.5
Typical 1σ main beam phase error	deg	10
Scanner range and resolution		
x, y, z range	mm	100
On-axis position resolution	μm	± 5
Alignment accuracy		
Lateral off-set in x and y	mm	< 0.1
Axial off-set in z	mm	< 0.2
Tilt around x and y	arcmin	< 5
Tilt around z	deg	< 0.1

For the software model, despite the absence of beam off-set in the focal plane, it turns out that on the sky, the two polarisation main beams are separated by $0.13''$, or 1.5% of the HPBW. This could be related to the differences in the non-uniform phase distribution arising from phase transformations of the optical coupling system front-end due to different aberration contributions. In the experimental case the beam separation angle is bigger (around 10% of the HPBW at 661 GHz, $0.77''$) than the software counterpart. This is due, most likely, to the two beam off-sets at the focal plane introduced by mechanical misalignments in the mirror block assembling procedure.

5. Conclusions

In this paper a comprehensive quasi-optical verification using simulation analysis and experimental assessment of the front-

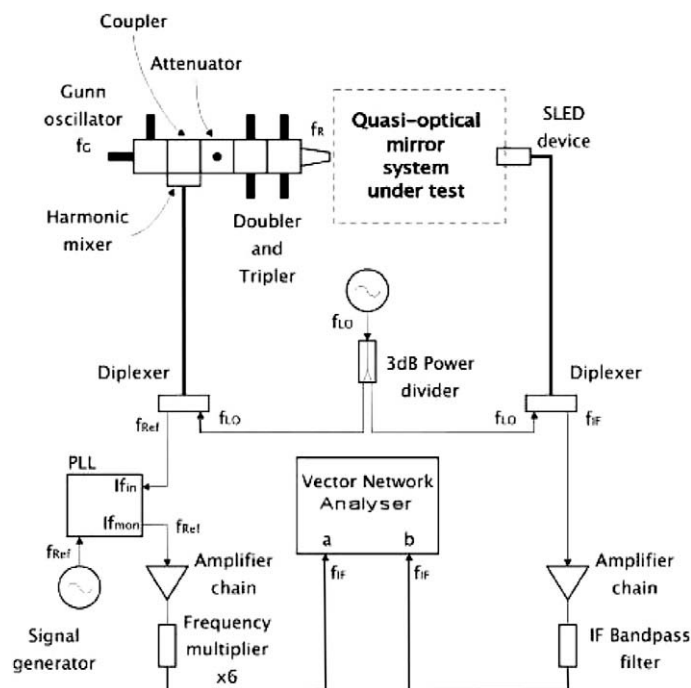


Fig. 5. Schematic of the custom made measurement set-up for the assessment of the ALMA band 9.

end system of the ALMA band 9 receiver is presented. The experimental near-field measurements in amplitude and phase have been supported by a high fidelity electromagnetic model set-up in GRASP. Remarkable agreement is illustrated in this paper with theoretical predictions compared to experimental measurements near the Cassegrain focal plane to the order of -40 dB at the band centre frequency of 668 GHz. The fundamental Gaussian fitting analysis carried out for both software and experimental data, allows full understanding of both data sets and is a very practical way to obtain the main beam behaviour in terms of lateral offset and tilt misalignment. The beam separation at the focal plane characterised by this Gaussian analysis for the experimentally measured data at the same location for both polarisation signals indicates a corresponding main beam deviation angle on the sky. An approximate method outlined without carrying out physical optics analysis on the telescope is comparable to the high fidelity results obtained involving physical optics analysis of the whole Cassegrain system. This potential beam separation artefact on the sky must be related to mechanical tolerancing and assembling errors of the optical system components. Overall the analysis and measurements between 600 and 720 GHz presented in this paper indicate the beneficial use of theoretical models based on physical optics for the design and assessment of such quasi-optical systems generally. The analysis presented also indicate that Band 9 will meet the overall ALMA requirements for optical performance and beam quality.

Acknowledgements

The authors wish to acknowledge the financial support of a Science Foundation Ireland (SFI) Research Frontiers Grant, and the European Community sixth Framework Programme under RadioNet R113CT 2003 5058187 JRA AMSTAR together with the Netherlands Astronomy Research School (NOVA).

Appendix A

A.1. Brief description of the measurement set-up

Experimental verification of the focal plane beam pattern, by amplitude and phase near-field beam measurements has been possible by means of a customised measurement set-up developed at SRON, Groningen. The system is capable of 2 D near-field scans with sufficient spatial resolution for measured frequencies from 600 to 720 GHz. In order to preserve phase information, the measurement system is based on radio heterodyne detection methods employing a vector network analyzer and external microwave circuitry generating the desired signal at band 9 frequencies. The block diagram of the measurement system is illustrated in Fig. 5. A scan is performed by a XYZ precision stage, which holds the Gunn oscillator chain, including the multipliers needed to achieve the desired RF frequency. The detector mounted at the back side of the mixer corrugated horn is a Super Lattice Electronic Device (SLED), which allows room temperature sub-harmonically pumped mixing [17]. The measurement method is based on mapping the complex field coupling coefficient between the field propagated through the optical system under test and the probe (open-ended rectangular waveguide) sampling on the scanning plane. The scanning system consists of three linear stages mounted orthogonally. The transmitter is then able to move on this plane within a square area, whose range and step resolution are listed in Table 5. The issue of aligning the scanning system with the front-end under test is solved by means of dedicated alignment reference devices mounted on the both device under test and the transmitter side. The reference devices are plane glass windows with cross-hairs

at the centre. These references are located in precise positions with respect to the device under test. Each of the cross-hairs centre locations is precisely determined in a coordinate system. The parallelism between the optics under test and the XY stages plane is ensured by theodolite autocollimation operations using the glass windows. The glass window on the optics under test is mounted perpendicular relative to the telescope axis. On the scanning system, the same concept of cross-hair references is adopted. In this case the normal to the glass window is parallel with the flared waveguide axis and the cross-hair centre position is precisely determined with respect to the centre of the flared guide aperture centre. In principle the two reference windows are placed parallel by a simultaneous theodolite autocollimation operation. Then, the scanner centre referenced by the flared waveguide centre, is related to the optics under test by mutually aligning the cross-hair centre of the alignment devices on the optical and the scanning system using the theodolite optical line of sight. It is also possible to calibrate the rotation around the theodolite line of sight by vertical alignment of an extra reference cross vertically located with respect to the other reference cross on the optics under test.

The precise alignment procedure is a vital operation for the quality and repeatability of the measurements and it allows measured and simulated data to be referenced to one single absolute coordinate system. Detailed comparison of simulations and measurements at a known plane are central to the verification procedure adopted for ALMA band 9. This precise alignment technique allows extremely accurate phase and amplitude measurements to be taken with exact information on the measurement plane.

References

- [1] H. Rudolf, M. Carter, A. Baryshev, The ALMA front end optics; system aspects and European measurement results, in: IEEE Transactions on Antennas and Propagation Special Issue on Optical and Terahertz Antenna Technology, November 2007.
- [2] L. King, Memo 52 - Preliminary optics design for the Millimeter Array Antennas, in: ALMA Memo Series, <<http://www.alma.nrao.edu/memos/>>, December 1988.
- [3] J. Cheng, D.T. Emerson, M.A. Gordon, J.B. Lugten, P.J. Napier (Chairman), J.M. Payne, W.J. Welch, D.P. Woody, Memo 145 - Antennas for the millimeter wave array, in: ALMA Memo Series, <<http://www.alma.nrao.edu/memos/>>, October 1995.
- [4] J. Cheng, Memo 182 - A 12-m antenna design for a joint US-European array, in ALMA Memo Series, <<http://www.alma.nrao.edu/memos/>>, September 1997.
- [5] J. Lugten, P. Napier (Chair), J. Biegling, J. Cheng, D. Emerson, M. Fleming, M. Holdaway, J. Kingsley, J. Lamb, J. Mangum, J. Payne, W. Welch, D. Woody, Memo 215 - A strawman optics layout for the MMA antenna, ver. 2, in: ALMA Memo Series, <<http://www.alma.nrao.edu/memos/>>, January 1998.
- [6] J.W.M. Baars, Memo 339 - Aspects of the antennas for the ALMA compact array (ACA), in: ALMA Memo Series, <<http://www.alma.nrao.edu/memos/>>, December 2000.
- [7] J.W. Lamb, Memo 246 - Optimized optical layout for MMA 12-m antennas, in: ALMA Memo Series, <<http://www.alma.nrao.edu/memos/>>, January 1999.
- [8] T.-S. Chu, An imaging beam waveguide feed, IEEE Transactions Antennas and Propagation AP-31 (4) (1983).
- [9] C.A. Balanis, Antenna theory, analysis and design, Interscience, Wiley, 2005.
- [10] P.F. Goldsmith, Quasioptical Systems, IEEE Press, 1998.
- [11] A. Baryshev, W. Wild, Memo 394 - ALMA band 9 optical layout, in: ALMA Memo Series, <<http://www.alma.nrao.edu/memos/>>, September 2001.
- [12] A.E. Siegman, Lasers, University Science Books, 1986.
- [13] H. Martin Derek, W. Bowden John, Long-wave optics, IEEE Transactions on Microwave Theory and Techniques 41 (10) (1993).
- [14] C.-Y.E. Tong, D.V. Meledin, D.P. Marrone, S.N. Paine, H. Gibson, R. Blundell, Near field vector beam measurements at 1 THz, IEEE Microwave and Wireless Components Letters 13 (2003) 235–236.
- [15] J. Kingsley, T. Andersen, ICD ALMA03006-04021-0001B. Technical report, ALMA Antenna and Front-End Group, October 2000.
- [16] J. Ruze, Antenna tolerance theory - a review, Proc. IEEE 54 (April) (1966) 633–640.
- [17] D.G. Pavel'ev, Yu. I. Koshurinov, V.P. Koshelets, A.N.Panin, V.L. Vaks, Superlattice harmonic mixer for submillimeter frequency synthesis, in: The Joint 29th International Conference on Infrared and Millimeter Waves and 12th International Conference on Terahertz Electronics, University of Karlsruhe, Karlsruhe, Germany, 2004.